Li and Na Storage Behaviours of MgFe$_2$O$_4$ Nanoparticles as Anode Materials for Lithium Ion and Sodium Ion Batteries

Jiaming Liu, Ruixiang Wang, Xiaocong Zhong, Kang Yan, Yuhu Li, Zhifeng Xu[*]

School of Metallurgy and Chemistry Engineering, Jiangxi University of Science and Technology, Ganzhou 341000, PR China
[*]E-mail: xzf_1@163.com

Porous structured MgFe$_2$O$_4$ particles were successfully prepared via a simple and low-cost route by sol–gel combustion synthesis. The final product was characterized by X-ray diffraction (XRD) and scanning electron microscopy (SEM). The average diameter of the prepared MgFe$_2$O$_4$ particles was found to be approximately 41 nm. When used as an anode material of lithium ion batteries (LIBs), MgFe$_2$O$_4$ showed an excellent cycling performance and a fairly high rate performance. The good Li storage performance can be attributed to the uniform porous structure without impurities that accommodates the strain due to the volume change in the charge/discharge cycles and expands the active area for lithium ion insertion. Additionally, the Na storage properties of MgFe$_2$O$_4$ as an anode material of sodium ion batteries were studied, and similar characteristics to those of LIBs were obtained during the discharge/charge cycles, with a high capacity in the initial discharge process but relatively moderate capacity retention compared to that found in the study of Li storage properties.

1. INTRODUCTION

Due to the increasing energy demand of portable electronics, electric vehicles (EV) and other rechargeable electronic devices, lithium ion batteries (LIBs) have become increasingly important in recent decades due to their high energy density and working potentials[1-5]. Graphite is commonly used as the anode active material for commercial LIBs because of its good Li reversibility. However, graphite is restricted by a low theoretical capacity (372 mAh g^{-1}), which hardly satisfies the needs of large-scale application in green grid energy storage[6, 7]. In addition, the low operating voltage of graphite (below 0.2 V vs. Li/Li$^+$) poses a safety risk due to the possible growth of lithium dendrites. To satisfy the demand

for next-generation LIBs, the development of novel electrode materials combining low cost, improved safety, high theoretical capacity, and easy synthesis is urgently required [8].

The spinel structure Fe-based binary metal oxide $MgFe_2O_4$ has been demonstrated to be very promising as an anode material for LIBs due to its low cost and the high theoretical Li storage capacity of 1072 mAh g^{-1}[9]. To date, intense efforts have been devoted to the synthesis of various morphologies of $MgFe_2O_4$ via various methods in order to obtain enhanced LIB performance. For example, $MgFe_2O_4$ nano-particles obtained by the sol–gel method show a specific capacity of 493 mAh g^{-1} after 50 cycles[10]. Hollow $MgFe_2O_4$ cubic particles synthesized by the self-sacrificial template method provide reversible capacity of 646 mAh g^{-1} over 100 cycles[11]. Other structures, such as vesicle-like $MgFe_2O_4$/graphene[12], quasispherical $MgFe_2O_4$[13] and so on were synthesized and their electrochemical properties were investigated. Nevertheless, the above methods involve relatively complicated processes and require long reaction   .

On the other hand, in light of the increasing energy demand for very-large-scale (stationary) electrical storage, sodium ion batteries (SIBs) have attracted considerable interest as a potential option for stationary electrical storage because sodium can be easily extracted on a worldwide scale. Furthermore, the working mechanism of SIBs is similar to that of LIBs[14, 15]. To develop effective anode materials for SIBs, many researchers have tended to focus on the materials that are feasible for use in LIB systems. Transition metal oxides, particularly ferrites, have been considered as promising SIB anode materials. Many exploratory studies on the behaviour of Fe-based oxides in Na storage have been carried out in the past few years[16-19].

In this paper, we report on the fabrication of $MgFe_2O_4$ particles for use as LIBs and SIBs anode materials through sol–gel combustion synthesis, which is an effective and rapid procedure with low energy consumption. It was found that $MgFe_2O_4$ particles exhibit excellent electrochemical performance characteristics as the anode material of LIBs. The high cycling stability and rate capability was ascribed to their porous structure, which can ease the effect of the volume change and enhance the electrical conductivity. Additionally, $MgFe_2O_4$ was used as a sodium ion battery anode material and its Na storage behavior was also investigated.

2. EXPERIMENTAL

2.1. Synthesis of MgFe₂O₄ particles

$MgFe_2O_4$ were synthesized using the sol–gel combustion method. All agents were of analytical grade and used without further purification. In a typical synthesis, $Mg(NO_3)_2\cdot 6H_2O$ (10 mmol) and $Fe(NO_3)_3\cdot 9H_2O$ (20 mmol) were dissolved in 60 mL deionized water. Then, 20 mmol of glycine was added into the above solution which was used as the fuel and ligand. The mixture solution was continuously stirred for a few minutes until glycine dissolved and obtained a homogeneous solution. The resultant solution was heated at 100 °C with constant magnetic stirring for 7 hours, transforming the solution into a xerogel. The xerogel was heated at 300 °C to burnt in a self-propagating combustion manner until form a loose powder. The powder was calcined in air at 700 °C for 2 hours with a heating rate of 3 °C min^{-1}.

2.2 Characterization

The sample is characterized by X-ray diffraction (XRD) using a Rigaku MiniFlex II X-ray diffractometer with Cu Kα radiation (λ = 0.154178 nm). Scanning electron microscope (SEM) micrographs were obtained on a FEI Nova NanoSEM 450 field emission scanning electron microscope.

2.3 Electrochemical measurements

The 70 wt% $MgFe_2O_4$ was mixed with a 10 wt% binder and 20 wt% conductive agent (super P) to form slurry. In which, the binders are polyvinylidene fluoride (PVDF) for Li-ions cells and sodium carboxymethyl cellulose (CMC) for Na-ion cells, respectively. The slurry was averagely loaded on Cu foil as the working electrode. And then, the electrode was dried in a vacuum oven at 80 °C overnight. The CR2016 coin cells were assembled in an Ar atmosphere glove box. The lithium foils were used as counter electrode in the Li-ion cells, and the Na-ion cells, where metallic Na played an analogous role. Different salts were dissolved in EC:DEC (2:1) to obtain 1 M $LiPF_6$ electrolyte for the Li-ion cells and 1 M $NaClO_4$ electrolytic solution for the Na-ion cells. A Celgard 2400 microporous polypropylene membrane and a glass fiber were used as the separator in Li and Na half cells, respectively. Galvanostatic charge-discharge cycling and rate performances of cells were performed in the range from 0.01 to 3.0 V (*vs*. Li/Li$^+$ or *vs*. Na/Na$^+$) with a Land BTI-40 (Wuhan, China) cell test system at room temperature.

3. RESULTS AND DISCUSSION
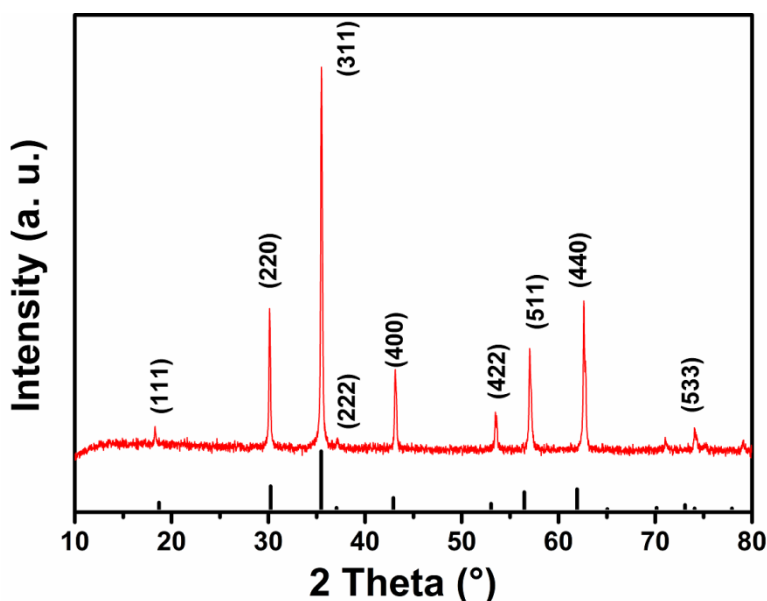
Figure 1. XRD pattern of $MgFe_2O_4$.

The crystal structure of $MgFe_2O_4$ was confirmed by XRD analysis. All of the diffraction peaks in the XRD patterns of the oxidation product can be readily indexed to spinel $MgFe_2O_4$ (JCPDS 89-

3084). There are no peaks of any other phases in the XRD pattern, indicating that the $MgFe_2O_4$ particles are pure single-phase materials. The obtained $MgFe_2O_4$ is highly crystalline, as indicated by the high peak intensity and small peak width. The average crystallite size of $MgFe_2O_4$ which is calculated according to the Scherrer's formula, is approximately 41 nm.

The morphology of the as-prepared $MgFe_2O_4$ powder was characterized by SEM microscopy, as shown in Fig. 2. It is observed that the material is composed of dendritic-like agglomerated particles. Fig. 2b shows that the material has a large number of pores. These pores can expand the active area that provides more contact between the electrode and the electrolyte.
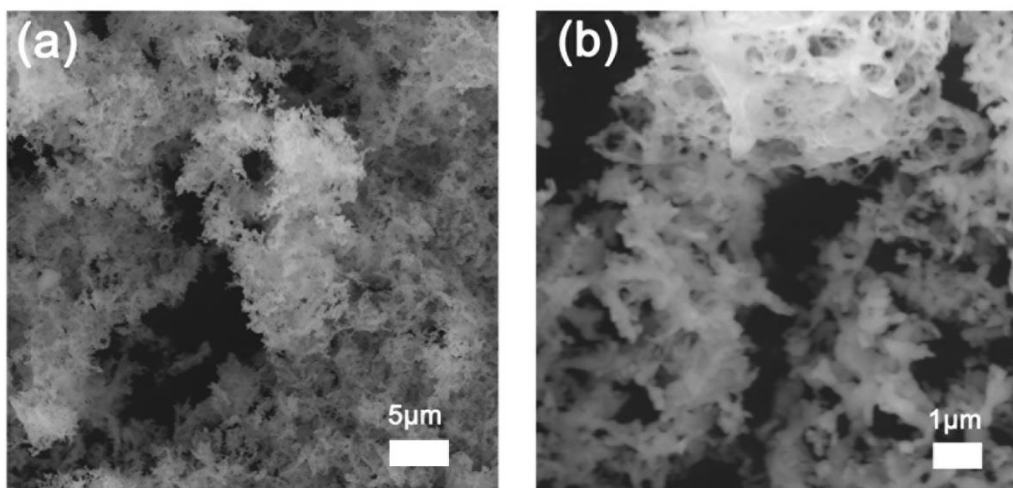
Figure 2. SEM images of $MgFe_2O_4$.

Fig.3 shows the discharge and charge curves of the $MgFe_2O_4$ electrodes in LIBs and SIBs at 200 and 100 mA g^{-1}, respectively. It is observed that the $MgFe_2O_4$ electrode in LIBs has a high capacity retention rate, while in SIBs, $MgFe_2O_4$ electrode capacity fades rapidly because of the large size of Na^+ ions, which leads to the high interface impedance, large volume expansion and slow ion diffusion[20]. As shown in Fig. 3a, there are two apparent plateaus at 0.79 and 0.37 V in the initial discharge process that are attributed to the reduction of Mg^{2+} and Fe^{3+} to Mg^0 and Fe^0 [9, 21]. The initial discharge and charge capacities are 1296.3 and 877.2 mAh g^{-1}, respectively, with a Coulombic efficiency of 67.7%. The large capacity loss is caused by the formation of a solid electrolyte interphase (SEI) layer and some irreversible Li_2O generation during the first discharge step[22]. The irreversible capacities do not increase or even decrease in the subsequent cycles. The discharge capacity is 869.2 mAh g^{-1} after 50th cycle, higher than that of the 2nd and 10th cycles. As shown in Fig. 3b, the initial discharge and charge capacities of the $MgFe_2O_4$ electrode in SIB are 863.7 and 616.6 mAh g^{-1}, respectively. However, the discharge capacity fades sharply in the subsequent cycles. The reversible specific capacity decreases to 468.8 in the 30th cycle.
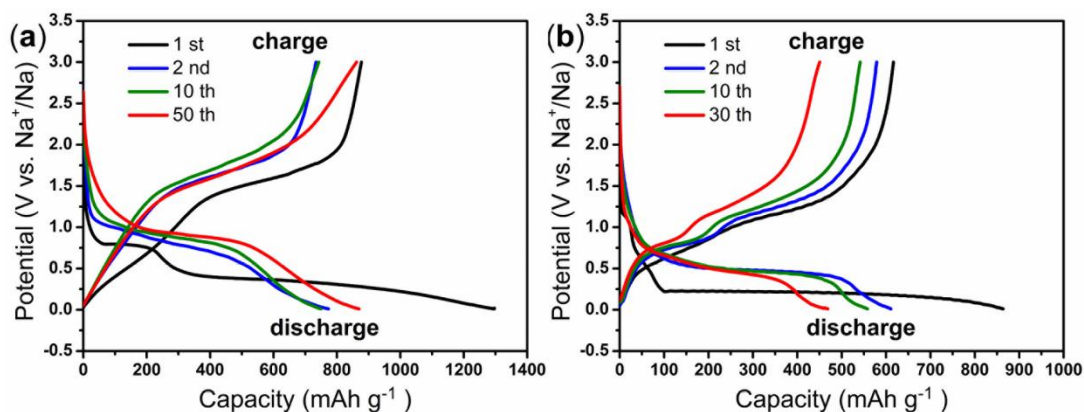
Figure 3. Discharge/charge voltage profiles of $MgFe_2O_4$ as anode material (a) in LIBs at a current density of 200 mA g^{-1}, (b) in SIBs at a current density of 100 mA g^{-1}.

Fig. 4 shows the cycling and rate performances characteristics of the $MgFe_2O_4$ electrode in LIBs. Fig. 4a presents the cycle stabilities of $MgFe_2O_4$ at 200 mA g^{-1}, 400 mA g^{-1} and 1000 mA g^{-1}, respectively. These curves have a similar trend with capacities first decreasing and then increasing and then finally decreasing again, and with Coulombic efficiency always higher than 95% except for the first cycle. The phenomenon of the gradual capacity increase has been extensively reported in transition metal oxide anode materials and is due primarily to structural the rearrangement with the reversible formation and decomposition of a polymeric-gel-like film on the active materials[23]. The polymeric-gel-like film is due to the kinetically activated electrolyte degradation, and acts a reservoir that stores excess Li^+ ions through a so-called "pseudo-capacitance-type behaviour"[24, 25]. In addition, the gel-like film can prevent the aggregation of active materials and mitigate the volumetric variation upon cycling[26]. The $MgFe_2O_4$ electrode exhibits outstanding reversible capacities of 1088.8 mAh g^{-1} at 200 mA g^{-1} after 100 cycles, 1191.7 mAh g^{-1} at 400 mA g^{-1} after 350 cycles and 850.2 mA g^{-1} at 1000 mA g^{-1} after 300 cycles. The high reversible capacity may be attributed to the presence of polymeric-gel-like films and interfacial lithium storage. Furthermore, porous particles with abundant interstitial space not only release the volume change pressure during the cyclic processes but also provide a larger area for Li^+ ions insertion.

Fig 4b shows the rate capability of the $MgFe_2O_4$ in LIBs at the current densities varying from 100 mA g^{-1} to 1600 mA g^{-1}. It is observed that the reversible capacity has not decreased significantly even at 1600 mA g^{-1}, still delivering 714.5 mA g^{-1}, indicating that the $MgFe_2O_4$ electrode can endure high current density cyclic pressure. With the current density recovering to 100 mA g^{-1}, $MgFe_2O_4$ electrode can deliver a capacity of 1011.3 mAh g^{-1}. This demonstrates that the $MgFe_2O_4$ electrode has good comprehensive electrochemical properties in a wide range of current densities.
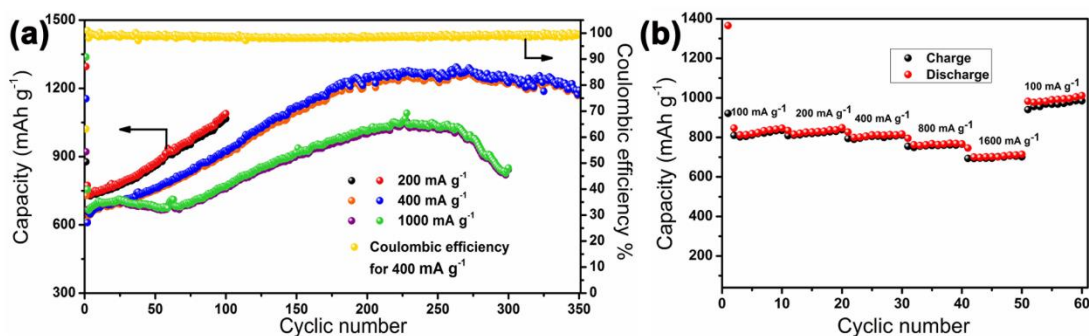
Figure 4. (a) Cycling performance of $MgFe_2O_4$ at different current densities in Li-ion batteries, (b) Rate performance of $MgFe_2O_4$ in LIBs.

The Na^+ storage behaviours of $MgFe_2O_4$ as an anode material of SIBs were also studied. The cycling property and Coulombic efficiency of the $MgFe_2O_4$ electrode with a current density of 100 mA g^{-1} are shown in Fig. 5(a). The Coulombic efficiency remains high but the specific capacity decreases significantly. The initial discharge capacity is 863.7 mAh g^{-1}, and the discharge capacity then decreases to 331.7 mAh g^{-1} after 50 cycles. The discharge capacity reduction indicates that the Na ions the collapse $MgFe_2O_4$ particle structure leading to an increase in the size of the nonreactive region. This can attribute to the large size and mass of the Na ion compared to the Li ion. Fig. 5(b) depicts the rate capability of the prepared $MgFe_2O_4$ electrode under various current densities in the range of 25 to 1000 mA g^{-1}. In the initial ten cycles, a steady trend is observed for the specific capacity. As the current density increases, the specific capacity gradually declines to 128 mhA g^{-1}. When the rate returns to 25 mA g^{-1}, the discharge capacity recovers to 429.4 mAh g^{-1} and then falls to 354.5 mAh g^{-1} in a few cycles, indicating the increase in the nonreactive region. The outstanding cycling stability characteristics of the porous $MgFe_2O_4$ electrode are summarized in Table 1 that also compares them with the cycling stability characteristics previously reported for other ferrites used as anodes for LIB and SIB systems.
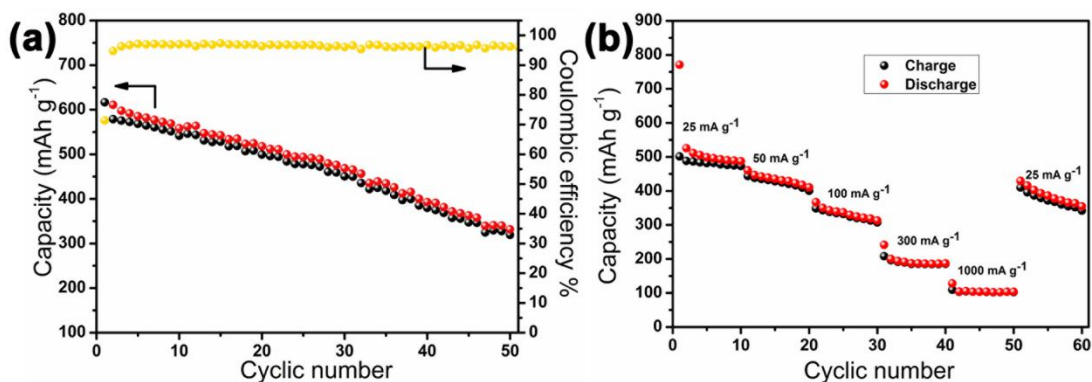
Figure 5. (a) Cycling performance of $MgFe_2O_4$ at a current density of 100 mA g^{-1} in SIBs, (b) Rate performance of $MgFe_2O_4$ in Na-ion batteries.

Table 1. Comparison of the results in this study with reported performance of ferrite as LIB and SIB anodes.

Sample	Cyclic stability	Reference
Porous $MgFe_2O_4$	1088.8 mAh g^{-1} at 200 mA g^{-1} (100 cycles)	Present
	1191.7 mAh g^{-1} at 400 mA g^{-1} (350 cycles)	work
	850.2 mAh g^{-1} at 1000 mA g^{-1} (300 cycles)	
	331.7 mAh g^{-1} at 50 mA g^{-1} (50 cycles)	
Nanostructured $MgFe_2O_4$	300 mAh g^{-1} at 0.2 mA cm^{-2} (10 cycles)	[9]
$MgFe_2O_4$ nanoparticles	493 mAh g^{-1} at 90 mA g^{-1} (50 cycles)	[10]
$MgFe_2O_4$/graphene nanocomposite	764.4 mAh g^{-1} at 42.9 mA g^{-1} (60 cycles)	[27]
Nano $MgFe_2O_4$	635 mAh g^{-1} at 100 mA g^{-1} (50 cycles)	[28]
3D network $MgFe_2O_4$/ graphene composite	1341 mAh g^{-1} at 500 mA g^{-1} (100 cycles)	[12]
$CuFe_2O_4$ nanotubes	816 mAh g^{-1} at 200 mA g^{-1} (50 cycles)	[29]
$ZnFe_2O_4$ microcages	824 mAh g^{-1} at 200 mA g^{-1} (100 cycles)	[30]
Rod-like $CuFe_2O_4$	281 mAh g^{-1} at 100 mA g^{-1} (20 cycles)	[18]
$MnFe_2O_4$/rGO composites	347.5 mAh g^{-1} at 50 mA g^{-1} (70 cycles)	[31]
$MnFe_2O_4$/rGO nanocomposite	258 mAh g^{-1} at 92.8 mA g^{-1} (50 cycles)	[32]

4. CONCLUSIONS

In summary, $MgFe_2O_4$ porous particles were successfully synthesized through a facile and effective sol-gel combustion method. For such a porous structure, the contact efficiency between electrode and electrolyte is improved, and the volume changes and internal strain are relieved. For the $MgFe_2O_4$ electrode in lithium ion batteries, the reversible capacities were 1088.8 mAh g^{-1} at 200 mA g^{-1} after 100 cycles and 1191.7 mAh g^{-1} at 400 mA g^{-1} after 350 cycles. At a high current density of 1000 mA g^{-1}, a reversible capacity of 850.2 mAh g^{-1} was maintained even after 300 cycles. The Na storage properties of the $MgFe_2O_4$, with such a porous structure used as the anode for sodium ion batteries, were also investigated. The $MgFe_2O_4$ electrode showed a high initial discharge capacity and an electrochemical process characteristic similar to those found for Li storage, albeit with capacity retention that is relatively moderate compared with that for lithium-ion batteries. To develop $MgFe_2O_4$ into a satisfactory candidate anode material for sodium ion batteries, some properties still must be improved through the modification of the microstructure.

References

1. J. B. GoodenoughandY. Kim, *Chem. Mater.*, 22 (2010) 587.
2. B. Dunn, H. KamathandJ. M. Tarascon, *Science*, 334 (2011) 928.
3. M. S. Whittingham, *Chem. Rev.*, 35 (2004) 4271.
4. B. ScrosatiandJ. Garche, *J. Power Sources*, 195 (2010) 2419-2430.
5. L. Q. Mai, Y. Gao, J. G. Guan, B. Hu, L. Xu, W. Jin, *Int. J. Electrochem. Sci.*, 4 (2009) 755.
6. B. DunnandJ. M. Tarascon, *Science*, 334 (2011) 928.
7. X. Fan, J. Shao, X. Xiao, L. Chen, X. Wang, S. LiandH. Ge, *J. Mater. Chem. A*, 2 (2014) 14641.
8. A. Manthiram, *J. Phys. Chem. Lett.*, 2 (2011) 176.
9. N. Sivakumar, S. R. P. Gnanakan, K. Karthikeyan, S. Amaresh, W. S. Yoon, G. J. ParkandY. S. Lee, *J. Alloys Compd.*, 509 (2011) 7038.
10. Y. Pan, Y. Zhang, X. Wei, C. Yuan, J. Yin, D. CaoandG. Wang, *Electrochim. Acta*, 109 (2013) 89.
11. Y. Guo, G. Qin, E. Liang, M. LiandC. Wang, *Ceram. Int.*, 43 (2017) 12519.
12. Y. Yin, W. Liu, N. HuoandS. Yang, *Acs Sustain. Chem. Eng.*, 5 (2016) 563.
13. H. LiuandH. Liu, *J. Electron. Mater.*, 43 (2014) 2553.
14. S. W. Kim, D. H. Seo, X. Ma, G. CederandK. Kang, *Adv. Energy Mater.*, 2 (2012) 710.
15. M. D. Slater, D. Kim, E. LeeandC. S. Johnson, *Adv. Funct. Mater.*, 23 (2013) 947.
16. Q. He, S. Gu, T. Wu, S. Zhang, X. Ao, J. YangandZ. Wen, *Chem. Eng. J.*, 330 (2017) 764.
17. Y. Liu, N. Zhang, C. Yu, L. JiaoandJ. Chen, *Nano Lett.*, 16 (2016) 3321.
18. X. Wu, W. Wu, Y. Li, F. LiandS. Liao, *Mater. Lett.*, 138 (2015) 192.
19. Z. J. Zhang, Y. X. Wang, S. L. Chou, H. J. Li, H. K. LiuandJ. Z. Wang, *J. Power Sources*, 280 (2015) 107.
20. Y. Liu, Y. Qiao, W. Zhang, P. Hu, C. Chen, Z. Li, L. Yuan, X. HuandY. Huang, *J. Alloys Compd.*, 586 (2014) 208.
21. X. Guo, X. Lu, X. Fang, Y. Mao, Z. Wang, L. Chen, X. Xu, H. YangandY. Liu, *Electrochem. Commun.*, 12 (2010) 847.
22. N. Huo, Y. Yin, W. Liu, J. Zhang, Y. Ding, Q. Wang, Z. ShiandS. Yang, *New J. Chem.*, 40 (2016) 7068.
23. Z. S. Wu, W. Ren, L. Wen, L. Gao, J. Zhao, Z. Chen, G. Zhou, F. LiandH. M. Cheng, *Acs Nano*, 4 (2010) 3187.
24. J. Wang, Q. Zhang, X. Li, B. Zhang, L. MaiandK. Zhang, *Nano Energy*, 12 (2015) 437.
25. J. Liu, J. Xiao, X. Zeng, P. Dong, J. Zhao, Y. ZhangandX. Li, *J. Alloys Compd.*, 699 (2017) 401.
26. Y. Yu, C. H. ChenandY. Shi, *Adv. Mater.*, 19 (2009) 993.
27. A.K. Rai, T.V. Thi, J. Gim, J. Kim, *Mater. Charact.*, 95 (2014) 259.
28. Y. Yin, B. Zhang, X. Zhang, J. Xu, S. Yang, *J. Sol-Gel Sci. Technol.*, 66 (2013) 540.
29. S. Peng, L. Li, M. Srinivasan, *J. Energy. Chem.*, 23 (2014) 301.
30. C. Wang, Y. Li, Y. Ruan, J. Jiang, Q.H. Wu, *Mater. Energy Today,* 3 (2017) 1
31. X. Zhang, T. Chen, D. Yan, W. Qin, B. Hu, Z. Sun, L. Pan, *Electrochim. Acta*, 180 (2015) 616.
32. P. Kollu, P.R. Kumar, C. Santosh, D.K. Kim, A.N. Grace, *RSC Adv.*, 5 (2015) 63304.